# Scleral Permeability Varies by Mouse Strain and Is Decreased by Chronic Experimental Glaucoma

Mary E. Pease,[1] Ericka N. Oglesby,[1] Elizabeth Cone-Kimball,[1] Joan L. Jefferys,[1] Matthew R. Steinhart,[1] Anthony J. Kim,[2] Justin Hanes,[1] and Harry A. Quigley[1]

[1]Glaucoma Center of Excellence and Center for Nanomedicine, Wilmer Ophthalmological Institute, Department of Ophthalmology, Johns Hopkins University School of Medicine, Baltimore, Maryland, United States
[2]Department of Neurosurgery, University of Maryland School of Medicine, Baltimore, Maryland, United States

Correspondence: Harry A. Quigley, Wilmer 122, Johns Hopkins Hospital, 600 North Broadway, Baltimore, MD 21287, USA; hquigley@jhmi.edu.

Submitted: September 24, 2013
Accepted: February 11, 2014

Citation: Pease ME, Oglesby EN, Cone-Kimball E, et al. Scleral permeability varies by mouse strain and is decreased by chronic experimental glaucoma. *Invest Ophthalmol Vis Sci.* 2014;55:2564–2573. DOI:10.1167/iovs.13-13327

**Purpose.** To determine differences in scleral permeability, as measured by diffusion of macromolecules, by using fluorescence recovery after photobleaching (FRAP), with reference to differences by mouse strain, scleral region, and the effect of experimental glaucoma.

**Methods.** In three mouse strains (B6, CD1, and B6 mice with mutation in collagen 8α2 [Aca23]), we used FRAP to measure the diffusion of fluorescein isothiocyanate–dextran, molecular weight 40 kDa, into a photobleached zone of sclera. Scleral regions near the optic nerve head (peripapillary) and two successively more anterior regions were compared. Sclera from mouse eyes subjected to chronically elevated intraocular pressure after bead injection into the anterior chamber were compared to fellow eye controls. FRAP data were compared against estimated retinal ganglion cell axon loss in glaucomatous eyes.

**Results.** Diffusion rates of dextran molecules in the sclera were significantly greater in Aca23 and B6 mice than in CD1 mice in a multivariate model adjusted for region and axial length ($P < 0.0001$). Dextran diffusion significantly decreased in glaucomatous eyes, and the decline increased with greater axon loss ($P = 0.0003$, multivariable model). Peripapillary scleral permeability was higher in CD1 than B6 and Aca23 mice ($P < 0.05$, multivariable model, adjusted by Bonferroni).

**Conclusions.** Measurement of the diffusion rates of dextran molecules in the sclera showed that glaucoma leads to decreased scleral permeability in all three mouse strains tested. Among mouse strains tested, those that were more susceptible to glaucomatous loss of retinal ganglion cells had a lower scleral permeability at baseline.

Keywords: glaucoma, mouse, experimental model, sclera, diffusion, permeability, photobleaching, dextran

Glaucoma is the second leading cause of world blindness and its principal risk factors include the effect of intraocular pressure (IOP) acting to decrease the number of retinal ganglion cells (RGCs). Intraocular pressure is a mechanical load that generates stress and strain in the sclera, which are magnified at the optic nerve head (ONH). The largest mechanical strains have been measured in in vitro inflation experiments in the peripapillary region, immediately adjacent to the ONH.[1] The sclera acts on the ONH, where axons of RGCs pass out of the eye, and suffers damage related to the effects of IOP.[2,3] Thus, the behavior of the sclera is highly relevant to glaucoma injury and its study may be useful in improved diagnosis as well as new therapeutic avenues.

The sclera comprises three-quarters of the human ocular circumference and is 75% to 90% collagen, with additional elastin fibrils and proteoglycans.[4,5] The scleral proteoglycans include heparin sulfate, chondroitin sulfate, dermatan sulfate, keratan sulfate, hyaluronan, aggrecan, and several small leucine-rich proteoglycans.[6,7] These may have important functional significance for the mechanical responses of the sclera.[8] Scleral thickness is greatest at the peripapillary zone, followed by the limbus, and is thinnest in midsclera.[9–12] The scleral collagen fibril diameter is larger[13] and varies more than in the cornea[14] or the lamina cribrosa of the ONH.[15] Scleral collagen fibrils, mostly type 1, are arranged in stacked and interwoven lamellae in which most fibrils course in parallel, with successive lamellae alternating in orientation. The mouse scleral lamellae are 41% anteroposterior, 20% oblique, and 15% circumferential collagen and 25% cellular lamellae of scleral fibroblasts.[16] In the peripapillary sclera, collagen and elastin fibrils are circumferentially oriented around the ONH to provide mechanical reinforcement against the large circumferential stress in this region.[17–23]

Human and murine scleral microanatomy differs with age and disease. In myopia[24,25] there is well-known scleral remodeling in response to defocus and form deprivation, extensively studied in animal models.[26–28] Both baseline scleral structure and its dynamic response seem to be important determinants of susceptibility to glaucoma damage.[1,12,20,29] Chronically elevated IOP in mice leads to decreases in nonfibrillar scleral elements, alterations in collagen lamellar orientation, a decrease in collagen fibril diameter, and increased cell division with a transition to the myofibroblast phenotype in scleral fibroblasts (Oglesby EN, unpublished observations,

2013).[16] Aca23 mice (mice of B6 background that are homozygous for mutation in collagen 8α2) are significantly protected against injury from experimental glaucoma,[30,31] while CD1 mice are considerably more susceptible to damage than B6 mice[32] and differ in important features of scleral anatomy and response.[9,33] Experimental glaucoma in mice increases axial length and width by 6% to 10%, with thinning of the peripapillary sclera and increased scleral stiffness in mechanical inflation testing. Types of mice that are more resistant to glaucoma injury have stiffer sclera in mechanical testing at baseline, and with chronic IOP increase, they undergo less midscleral thinning and resist axial elongation better.[9,16]

Recent experimental results suggest that an important change in mouse glaucomatous eyes is loss of the interfibrillar matrix as the eye elongates and stiffens.[16] While modeling of scleral biomechanical behavior has included parameters that stand in for the matrix, its actual features have not been studied in detail in glaucoma models. Proteoglycans within connective tissues are known to be important mediators of the biomechanics of fibrillar elements. Fibroblasts of the sclera make up 25% of its volume in histologic preparations and are known to actively modify both fibrils and matrix.[26,34] To study the physiology of the scleral matrix, we developed a method based on the technique of fluorescence recovery after photobleaching (FRAP) to assess the diffusion of large, labeled molecules in the sclera in vitro. This method was used to compare the diffusion rates of 40-kDa dextran molecules in three scleral regions in three strains of mice, each of which had undergone experimental glaucoma in one eye.

## Methods

### Animals

Animals were treated in accordance to the ARVO Statement for Use of Animals in Ophthalmic and Vision Research, with protocols approved and monitored by the Johns Hopkins University School of Medicine Animal Care and Use Committee. A total of 34 mice underwent FRAP testing. Three strains of mice at 3 to 4 months of age were studied in one or both eyes: 9 C57BL/6 mice (B6 from Jackson Laboratories, Bar Harbor, ME, USA), 9 CD1 mice (Charles River Laboratories, Wilmington, MA, USA), and 10 Aca23 mutant mice (base strain B6), previously described.[30] In addition, six CD1 mice at 15 months of age were studied. The word "strain" is used in this report generally to indicate a particular type of mouse, not in the sense of mechanical stress–strain, except where specifically discussing biomechanical behavior.

### Intraocular Pressure Measurement

For IOP measurement, animals were anesthetized by inhalation of isoflurane, using the $RC^2$–Rodent Circuit Controller (VetEquip, Inc., Pleasanton, CA, USA). This instrument delivers 2.5% isoflurane mixed with oxygen via nose cone. Two minutes after the animal was sedated, IOP measurements were made by using the TonoLab tonometer (TioLat, Inc., Helsinki, Finland), recording the mean of six readings with optimal reliability score. We measured baseline IOP before injection, at 10 minutes after injection, and weekly to euthanasia at 6 weeks after initiation of chronic IOP elevation by bead injection.

### Bead Injections for Glaucoma

Mice were anesthetized by an intraperitoneal injection of 50 mg/kg ketamine, 10 mg/kg xylazine, and 2 mg/kg acepromazine and received topical anesthesia of 0.5% proparacaine hydrochloride eye drops (Akorn, Inc., Buffalo Grove, IL, USA). The bead injection protocol used was the 4 + 1 method, in which we sequentially injected the following through a glass cannula (tip diameter, 50 μm) connected by polyethylene tubing to a Hamilton syringe (Hamilton, Inc., Reno, NV, USA): 2 μL 6-μm-diameter beads, then 2 μL 1-μm-diameter beads (both from Polybead Microspheres; Polysciences, Inc., Warrington, PA, USA), followed finally by 1 μL viscoelastic compound (10 mg/mL sodium hyaluronate, Healon; Advanced Medical Optics, Inc., Santa Ana, CA, USA).[33] The approximate final concentration in injections is $3 \times 10^6$ beads per μL for 6-μm beads and $1.5 \times 10^7$ beads per μL for 1-μm beads.

### Fluorescence Recovery After Photobleaching

Mice were deeply anesthetized by using an intraperitoneal cocktail of ketamine, xylazine, and acepromazine (50, 10, and 2 mg/kg, respectively) and the eyes were enucleated before euthanasia by exsanguination. Both eyes of each animal were placed in phosphate-buffered saline (PBS) and cleaned of extraocular tissues. Axial length and width measurements were taken by using a digital caliper (Instant Read Out Digital Caliper; Electron Microscopy Sciences, Hatfield, PA, USA) as described below. The posterior sclera was separated from anterior structures and the retina and choroid were removed with a brush. The dural sheath and optic nerve stump were cut off flush with the sclera before blocking into two flat mounts (Fig. 1).

Three regions of the superior and inferior sclera were studied: the immediate peripapillary zone (R1), a zone 0.75 mm anterior to the ONH margin superiorly (R2/3), and a zone 1.5 mm inferior to the ONH margin (R4). Sclera from glaucoma and fellow control eyes was placed in fluorescein isothiocyanate–dextran (FITC-dextran) solution, molecular weight 40 kDa (FD-40; Sigma-Aldrich Corp., St. Louis, MO, USA), at a concentration of 1 mg/mL in PBS and incubated in the dark for 90 minutes. Samples were mounted on a slide outer sclera side up and coverslipped with an additional 25 μL FITC-dextran solution. Slides were sealed with clear nail polish and kept in the dark until imaging shortly after.

In brief, FRAP quantifies the two-dimensional diffusion of fluorescently labeled molecules within cells or tissues.[35,36] Confocal FRAP image sets consist of a time series in the following sequence: (1) baseline image, (2) exposure to laser energy to bleach the designated region, and (3) sequential, postbleach scans to quantify re-entry of unquenched dye from surrounding tissues into the bleached region. Intensity of fluorescence over time into the bleached area is modeled as a bleach recovery function, whose half-time is used to calculate a diffusion coefficient, or tissue diffusivity of fluorescently labeled molecules. We used the Zeiss LMS710 NLO (Zeiss, Inc., New York, NY, USA) with its 488-nm laser at 2% power, a 488 main beam splitter and 415 to 735 band pass, and the Plan-Apochromat 63×/1.40 oil objective lens. The optimal pre- and postbleach gain varied from 650 to 850 among specimens, but was maintained at one setting for the replicates at a given position for both right and left eyes of the same animal. The bit depth used was 12, providing 0 to 4095 levels of intensity. The imaging window was 100 μm × 50 μm and the bleach zone was a circle, 5 nm in diameter, with a similar-sized bleach reference circle. Data collection consisted of two prescans at 2% power, followed by 100 iterations of 100% laser power directed at the bleach zone, followed by 78 more full scans taken during the next 30 seconds. Images were centered at the midpoint between the inner and outer sclera. In each region, four to six bleaching replicates were conducted and their results were averaged.

Analysis of fluorescent intensity data used Zen 2010 LSM710 software, release 6.0 (Zeiss, Inc.), fitting an exponen-

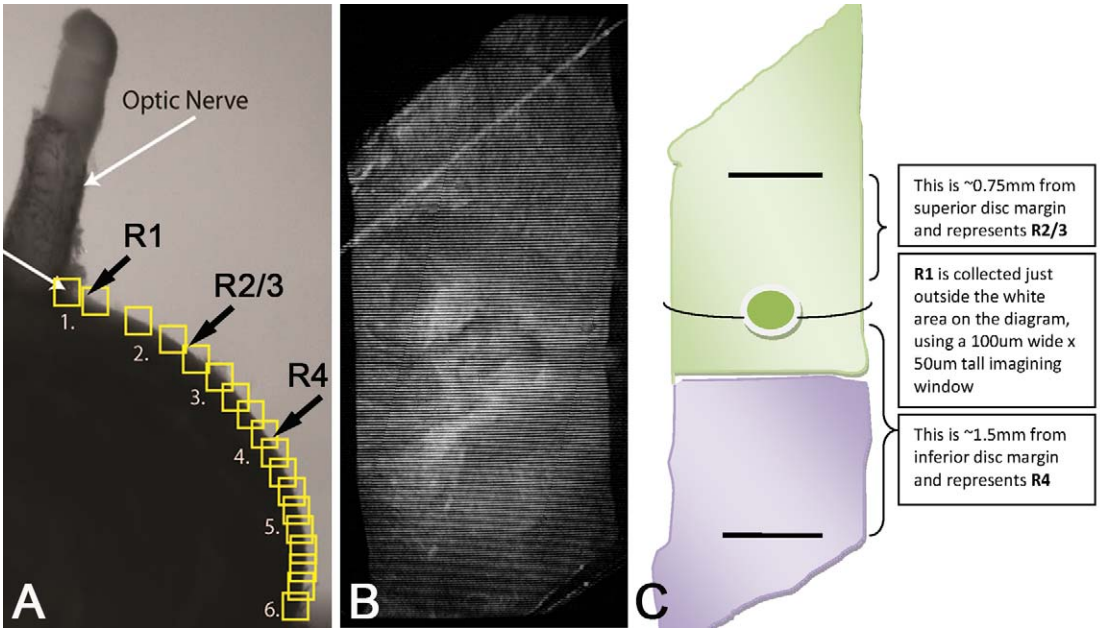


FIGURE 1. Schematic of tissue preparation and sampling locations. The locations on the intact mouse eye that correspond to our sampling locations are marked (**A**). The retinal wholemount (**B**) was divided into two pieces to aid flattening, and its schematic (**C**) demonstrates where R1, R2/3, and R4 were located on the resulting two flat mounts.

tial function to the fluorescence recovery data, which was calculated by comparing the percentage bleach of mobile and immobile fractions, producing a half-time to bleach recovery (t ½), which was then used as the primary outcome variable (Fig. 2).

Before using the specific dextran selected, we tested fluorescent polystyrene nanoparticles with bio-inert polyethylene glycol (PEG) coating (20-, 40-, and 100-nm PS-PEG), quantum dots (15–20 nm nontargeted Qdot 655; Invitrogen, Carlsbad, CA, USA), and different sized FITC-dextrans (15, 40, and 150 kDa; Sigma-Aldrich Corp.). The PS-PEG nanoparticles and Qdots were unable to diffuse in sclera, most likely because the particle sizes are too large compared to the pore size of the sclera. The other FITC-dextrans were also not suitable for our experiment. The larger 150-kDa dextran (8.5 nm) showed a fluorescence recovery that never reached its initial prebleach fluorescence level, probably owing to its larger hydrodynamic size (8.5 nm). The smaller 15-kDa FITC-dextran (2.3 nm) could not be completely photobleached, since a significant fraction quickly diffused back into the bleach region during photobleaching. The 40-kDa FITC-dextran provided a good balance between complete photobleaching and best fluorescence recovery.

## RGC Axon Loss Quantification

The optic nerve was removed from the globe and fixed by immersion in 4% paraformaldehyde in 0.1 M sodium phosphate buffer (pH = 7.2). After initial paraformaldehyde fixation, the optic nerve was removed and postfixed in 1% osmium tetroxide, dehydrated in alcohol, and stained with 1% uranyl acetate in 100% ethanol for 1 hour. Nerves were embedded in epoxy resin and 1-μm cross-sections were cut. To assess RGC damage, we estimated axon loss in optic nerve cross-sections by a semiquantitative grading system. An observer masked to the protocol (glaucoma or fellow eye) examined sections by phase contrast microscopy and gave one of five grades: normal, <10% axon damage, 10% to 25% damage, 25% to 50% damage, or >50% damage. Owing to the need to study the remainder of the eye without fixation, perfusion of aldehyde could not be performed. Perfusion fixation is required for detailed quantitative axon counting.[37]

## Axial Length and Width Measurement

The globes were removed and IOP was set at 15 mm Hg with a needle connected to a fluid-filled reservoir to produce standard conditions for axial length and width measurement. The measurements were performed with a digital caliper (Instant Read Out Digital Caliper; Electron Microscopy Sciences). The length was measured from the center of the cornea to a position just temporal to the optic nerve, and both nasal-temporal width and superior-inferior width were measured at the largest dimension at the equator, midway between the cornea and optic nerve.

## Statistical Analysis

The primary outcome parameter was the half-time to recovery, with larger values of t ½ indicating slower diffusion. For estimation of the effect of experimental glaucoma, we calculated the paired difference between the t ½ in each glaucomatous eye and that in its fellow eye. A shorter t ½ would indicate a greater permeability. Mean and standard deviation for t ½ were calculated for relevant subgroups. To carry out regression analysis, a natural log transformation was made of the t ½ data. Greater diffusion in glaucomatous eyes than control values indicated that the bead-injected eyes became more porous with treatment. The estimated effect of various factors on diffusion and the associated *P* values were obtained by using generalized estimating equation models, which take into account correlations among repeated measurements on a single mouse eye. This was appropriate because we studied three areas of the sclera from most eyes. The working correlation matrix for the repeated measurements was assumed to have an autoregressive structure, in which

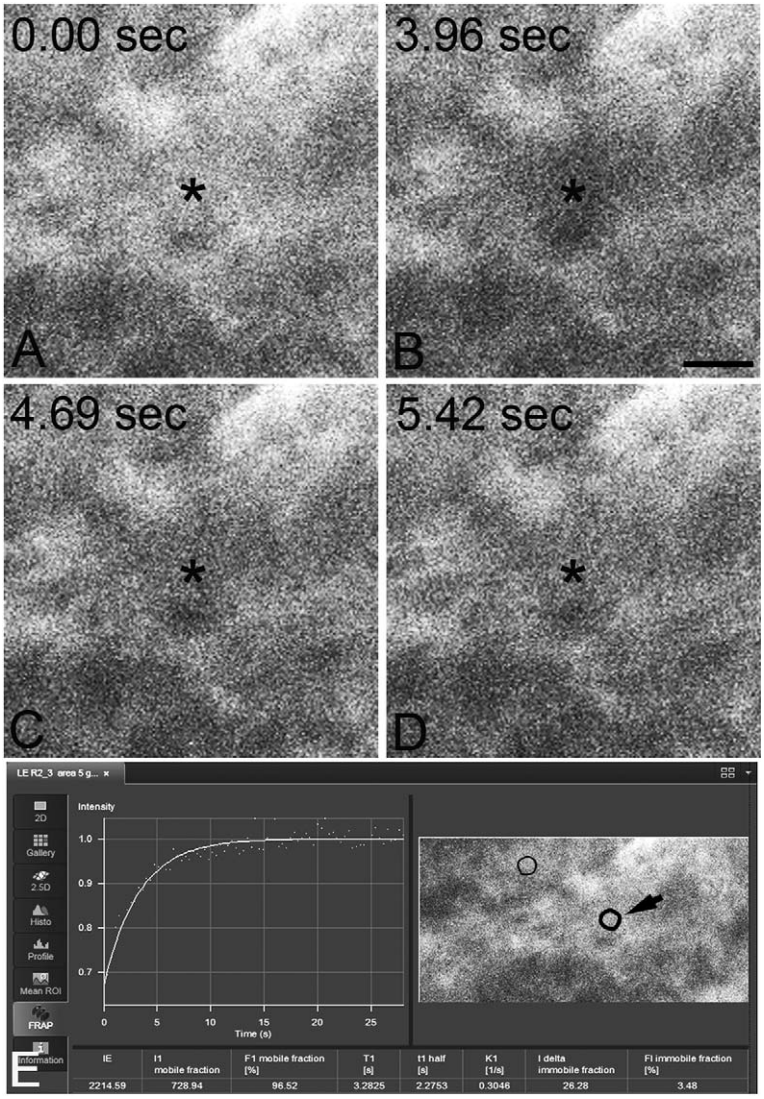


**Figure 2.** Sample bleach and recovery. (**A–D**) were taken from a subportion of the image, which included the bleach spot at baseline (0.00 seconds), immediately after bleach (3.96 seconds), and two subsequent scans during recovery (4.96 and 5.43 seconds). The *asterisk* indicates the approximate center of the 5-nm bleach spot. A screenshot of the Zeiss FRAP curve fitting and the entire imaging window at baseline are visible in (**E**). The *arrow* points to the bleach region of interest, the other *circle* is the reference region of interest used to correct for photobleaching across the entire imaging window during pre- and postbleach acquisitions. *Scale bar*: 5 nm.

measurements from closer regions have higher correlation. Bonferroni adjustments were made for multiple comparisons. For axial length, median, as well as mean and standard deviation, was calculated for each of four groups of control eyes: B6, CD1 young, CD1 old, and Aca23. Groups were compared by using analysis of variance with Dunn's test for multiple comparisons.

## Results

### Control Scleral Permeability by Mouse Strain

The t ½ of 40-kDa dextran molecules in the sclera in the control, untreated sclera in Aca23 mutant mice, and B6 mice was lower (faster recovery, indicating greater permeability) than in CD1 mice (Table 1; includes young CD1 but not older

**Table 1.** Mean Half-Time to Recovery in Sclera Among Control and Glaucomatous Eyes by Region and Mouse Strain

| | B6 | | CD1 Young | | Aca23 | |
|---|---|---|---|---|---|---|
| **Region** | **Control** | **Glaucoma** | **Control** | **Glaucoma** | **Control** | **Glaucoma** |
| Region 1 | 2.616 ± 1.283 | 2.843 ± 1.456 | 4.134 ± 1.246 | 4.084 ± 1.463 | 1.876 ± 0.591 | 1.767 ± 0.728 |
| Region 2/3 | 1.610 ± 0.254 | 1.923 ± 0.519 | 2.207 ± 0.448 | 2.161 ± 0.316 | 2.206 ± 0.723 | 2.405 ± 1.061 |
| Region 4 | 2.061 ± 0.539 | 2.124 ± 0.670 | 2.284 ± 0.500 | 1.902 ± 0.206 | 1.954 ± 1.172 | 2.803 ± 1.127 |

The values are mean ± standard deviation, with 8 to 10 samples per region for each control and glaucoma group.

**Table 2.** Multivariable Model for the Effect of Strain on Log Half-Time Among Control Eyes Adjusting for Region and Axial Length ($N = 27$)

| Factor | Estimated Mean Half-Time | Regression Parameter Estimate (95% CI) | *P* Value | Categories Different at Adjusted $P \leq 0.05$ (Bonferroni) |
|---|---|---|---|---|
| Strain | | | | |
| B6 (R) | 1.949 | 0 | | B6, CD1 |
| CD1 | 2.692 | 0.323 (0.154, 0.492) | <0.0001 | CD1, Aca23 |
| Aca23 | 1.866 | −0.043 (−0.268, 0.182) | | |

Log, natural logarithm transformation; CI, confidence interval; R, reference category.

**Table 3.** Mean Axial Length Among Control Eyes by Mouse Strain

| Group | *N* | Mean ± SD | Median |
|---|---|---|---|
| B6 | 9 | 3.37 ± 0.090 | 3.35 |
| CD1 young | 9 | 3.43 ± 0.089 | 3.46 |
| Aca23 | 9 | 3.53 ± 0.071 | 3.53 |
| CD1 old | 4 | 3.58 ± 0.171 | 3.55 |

SD, standard deviation.

CD1 mice). These pairwise differences were highly significant in a univariate model (overall $P < 0.0001$) and in a multivariate model adjusted for region and axial length (overall $P < 0.0001$; Table 2).

*Axial length* was of interest as a modifier of permeability because baseline axial length differs significantly among the three strains of mice studied. B6 mice have the shortest axial length, while that of CD1 mice is intermediate and Aca23 mice have the longest eyes ($P = 0.002$, one-way ANOVA, pairwise difference of B6 and Aca23, $P < 0.01$ and CD1 and Aca23, $P < 0.05$, Dunn's multiple comparisons test; Table 3). In models including all three strains of mice, there was no significant relationship between t ½ and axial length. However, in data comparing younger and older CD1 mice, effects of axial length were identified (see below).

## Region of Sclera

Univariate analysis of t ½ among control eyes in all three strains found a significant relationship between the region of sclera and t ½ ($n = 27$ eyes, $P = 0.01$; Table 4). Permeability was least (longest t ½) in the peripapillary sclera (region 1) compared to either of the more anterior regions.

A multivariate model of the log-transformed t ½, with all three strains included, showed that there were significant differences by strain and region, with higher t ½ (slower recovery indicating less permeability) in CD1 than B6 and Aca23 mice in the peripapillary region (R1) and higher t ½ (lower diffusion) in CD1 than in B6 mice in region 2/3 (Table 5).

**Table 4.** Univariate Models for Log Half-Time to Recovery Among Control Eyes

| Factor | *N* | Estimated Mean Half-Time | Regression Parameter Estimate (95% CI) | *P* Value | Categories Different at Adjusted $P \leq 0.05$ (Bonferroni) |
|---|---|---|---|---|---|
| Strain | | | | | |
| B6 (R) | 27 | 1.932 | 0 | <0.0001 | B6, CD1 |
| CD1 | | 2.688 | 0.330 (0.155, 0.505) | | CD1, Aca23 |
| Aca23 | | 1.870 | −0.033 (−0.254, 0.188) | | |
| Region | | | | | |
| Region 1 (R) | 27 | 2.564 | 0 | 0.01 | Region 1, Region 2/3 |
| Region 2/3 | | 1.929 | −0.285 (−0.482, −0.087) | | Region 1, Region 4 |
| Region 4 | | 1.977 | −0.260 (−0.444, −0.076) | | |

**Table 5.** Multivariable Model for Effect of Strain by Region on Log Half-Time to Recovery Among Control Eyes

| Factor | Estimated Mean Half-Time | Regression Parameter Estimate (95% CI) | *P* Value From GEE Model | Categories Different at Adjusted $P \leq 0.05$ (Bonferroni) |
|---|---|---|---|---|
| Strain in region 1 | | | | |
| B6 (R) | 2.35 | 0 | <0.0001 | B6, CD1 |
| CD1 | 3.982 | 0.527 (0.162, 0.893) | | CD1, Aca23 |
| Aca23 | 1.787 | −0.274 (−0.638, 0.090) | | |
| Strain in region 2/3 | | | | |
| B6 (R) | 1.594 | 0 | 0.001 | B6, CD1 |
| CD1 | 2.17 | 0.309 (0.143, 0.475) | | |
| Aca23 | 2.075 | 0.264 (−0.030, 0.558 ) | | |
| Strain in region 4 | | | | |
| B6 (R) | 2.004 | 0 | 0.26 | None |
| CD1 | 2.248 | 0.115 (−0.087, 0.317) | | |
| Aca23 | 1.742 | −0.141 (−0.473, 0.192 ) | | |

GEE, generalized estimating equation.

Table 6. Mean Half-Time Among CD1 Control Eyes by Age and Region

| | Age | | | |
|---|---|---|---|---|
| | Young | | Old | |
| Region | N | Mean ± SD | N | Mean ± SD |
| Region 1 | 9 | 4.134 ± 1.246 | 6 | 4.932 ± 1.045 |
| Region 2/3 | 9 | 2.207 ± 0.448 | 6 | 2.257 ± 0.298 |
| Region 4 | 8 | 2.284 ± 0.500 | 6 | 3.648 ± 0.833 |
| All regions | 9 | 2.898 ± 0.214 | 6 | 3.612 ± 1.347 |

## Age Effect

We compared two age groups of control CD1 mouse eyes for t ½ in the sclera: 40-kDa dextran diffused more slowly in older CD1 mice at 15 months of age (less permeability) than in younger CD1 mice at 4 months of age ($P = 0.0005$, univariate regression; Tables 6, 7). Furthermore, t ½ was lower in the peripapillary region (R1) than in the two more anterior regions ($P < 0.0001$, univariate regression). Overall, axial length was not significantly related to t ½ in a univariate model (Table 7). But, in a multivariate regression model including age, region, and axial length, a statistically significant interaction was found in the effects of age, axial length, and region on t ½ (Table 8). Diffusion of dextran molecules in the sclera was reduced in older mice and in the peripapillary region, and was greater in mice with longer eye axial length (when adjusted for age). However, older CD1 eyes had longer axial length and yet lower t ½, explaining why axial length without adjustment for age was not related to t ½ in a univariate model.

## Effect of Glaucoma on t ½ in the Sclera

Glaucomatous eyes showed a consistent decrease in t ½ within the sclera as the amount of estimated damage to the RGC caused by glaucoma increased (Table 9; Fig. 3). Whether considered as five levels of damage or in three groups indicated by normal, less than 25% damage, and 25% damage or more, there was a significant trend to lower t ½ with greater axon loss (univariate regression of pairwise glaucoma versus control eyes, Table 10). In addition, multivariable models comparing glaucoma to control eyes pairwise found significantly greater t ½ with increasing glaucoma damage, whether considered in three damage groups or with percentage axon loss as a continuous variable (Table 11).

# Discussion

Our quantitative measurements of scleral permeability showed differences among strains of mice, differences by region of the sclera, and a decrease in permeability after experimental glaucoma in mice. The t ½ of 40-kDa dextran molecules in the sclera was shorter in both the typical B6 strain and the B6-based Aca23 mutants than in CD1. Interestingly, the rank order of scleral permeability among these three mouse strains matched the rank order of susceptibility to experimental glaucoma damage among these three types of mice. In previous reports, we have shown that the Aca23 mutants, which had the greatest permeability estimates here, are the strain that is most resistant to glaucoma damage, while the CD1 mice with lowest permeability are most susceptible to glaucoma injury, with the B6 mice intermediate in both measures.[31–33] This finding lends further credence to the potential role of the state of the sclera as a factor in glaucoma

Table 7. Univariate Models for Log Half-Time Among CD1 Control Eyes

| Factor | Estimated Mean Half-Time | Regression Parameter | | P Value From GEE Model |
|---|---|---|---|---|
| | | N | Estimate (95% CI) | |
| Age | | | | |
| Young (R) | 2.636 | 16 | 0 | 0.0005 |
| Old | 3.244 | | 0.208 (0.091, 0.324) | |
| Region | | | | |
| Region 1 (R) | 4.303 | 16 | 0 | <0.0001 |
| Region 2/3 | 2.198 | | −0.672 (−0.812, −0.532) | |
| Region 4 | 2.749 | | −0.448 (−0.648, −0.249) | |
| Axial length, mm, per unit increase | ——— | 13 | 0.217 (−0.217, 0.651) | 0.33 |

Table 8. Multivariable Model for Log Half-Time Among CD1 Control Eyes ($N = 13$)

| Factor | Estimated Mean Half-Time | Regression Parameter Estimate (95% CI) | P Value From GEE Model | Categories Different at Adjusted $P \leq 0.05$ (Bonferroni) |
|---|---|---|---|---|
| Region in young | | | | |
| Region 1 (R) | 3.909 | 0 | <0.0001 | Region 1, region 2/3 |
| Region 2/3 | 2.13 | −0.607 (−0.775, −0.438) | | Region 1, region 4 |
| Region 4 | 2.214 | −0.569 (−0.828, −0.309) | | |
| Region in old | | | | |
| Region 1 (R) | 4.942 | 0 | <0.0001 | Region 1, region 2/3 |
| Region 2/3 | 2.478 | −0.690 (−0.985, −0.395) | | Region 2/3, region 4 |
| Region 4 | 4.193 | −0.164 (−0.501, 0.172) | | |

**Table 9.** Mean Half-Time Among Glaucomatous Eyes by Level of Damage and Mouse Strain

| Treatment Level of Damage | B6 | | CD1 | | Aca23 | | All Strains | |
|---|---|---|---|---|---|---|---|---|
| | *N* | Mean ± SD | *N* | Mean ± SD | *N* | Mean ± SD | *N* | Mean ± SD |
| Control | 9 | 2.076 ± 0.875 | 9 | 2.898 ± 1.214 | 9 | 2.012 ± 0.844 | 27 | 2.328 ± 1.060 |
| Glaucoma | | | | | | | | |
| Normal | 3 | 1.881 ± 0.472 | 0 | ——— | 4 | 2.186 ± 1.039 | 7 | 2.055 ± 0.841 |
| <10% | 3 | 1.863 ± 0.489 | 2 | 2.772 ± 1.550 | 3 | 2.524 ± 1.131 | 8 | 2.338 ± 1.096 |
| 10%–25% | 1 | 3.940 ± 1.939 | 3 | 2.806 ± 1.600 | 1 | 1.300 ± 0.512 | 5 | 2.731 ± 1.671 |
| 25%–50% | 1 | 2.493 ± 1.142 | 2 | 2.782 ± 1.407 | 0 | ——— | 3 | 2.686 ± 1.259 |
| >50% | 0 | ——— | 1 | 2.597 ± 0.391 | 1 | 3.197 ± 0.501 | 2 | 2.897 ± 0.519 |
| Glaucoma | | | | | | | | |
| Normal | 3 | 1.881 ± 0.472 | 0 | ——— | 4 | 2.186 ± 1.039 | 7 | 2.055 ± 0.841 |
| <25% | 4 | 2.382 ± 1.319 | 5 | 2.792 ± 1.524 | 4 | 2.218 ± 1.133 | 13 | 2.489 ± 1.139 |
| ≥25% | 1 | 2.493 ± 1.142 | 3 | 2.720 ± 1.133 | 1 | 3.197 ± 0.501 | 5 | 2.770 ± 1.006 |

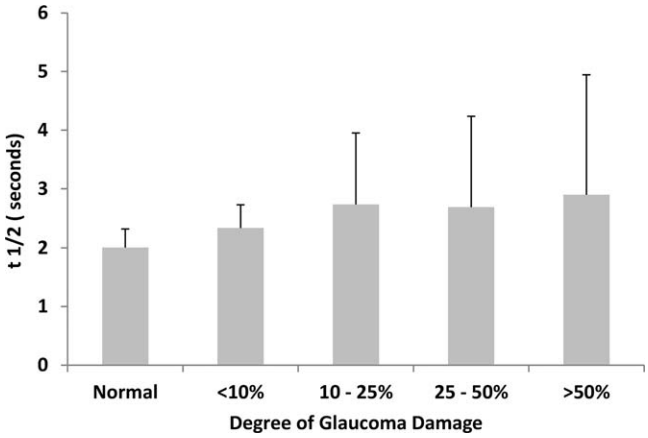


**Figure 3.** Permeability (half-time) by degree of glaucoma injury. Scleral permeability decreases (t ½ increases) significantly as glaucoma damage increases.

susceptibility. In addition, there was a significant, monotonic decrease in scleral permeability with greater glaucoma damage in experimental mice in this study. If lower scleral permeability is associated with greater susceptibility, then the decreased permeability that was induced by experimental glaucoma in our data would be a detrimental trend, potentially inducing a vicious cycle.

The peripapillary sclera is vitally important in glaucoma injury, since it has greater IOP-induced mechanical strain than other scleral zones. Experimental models of ocular biomechanics point to the importance of the peripapillary area in the effect of IOP on the ONH and RGC axons passing through it.[29,38] Our findings showed that the two standard mouse strains (B6 and CD1) have a lower peripapillary scleral permeability than the more anterior regions of the same eyes. In multivariate modeling, where region and strain are included, the control peripapillary sclera had a longer t ½ in CD1 mice than in the two B6-based strains. The lower permeability in a local region known to be most important to glaucoma injury seems to indicate that the greater strain in this zone has structural and physiological consequences that merit further study.

Older age is associated with increased glaucoma susceptibility in human open-angle glaucoma.[39] In this study, we found that there was lower permeability to dextran in older CD1 than in younger CD1 mice. Related measures of scleral permeability, namely hydraulic conductivity and permeability to albumen, have been reported to decline with age in human eyes,[40,41] and these findings are consistent with our permeability data. We have recently found that older CD1 mice are more susceptible

**Table 10.** Univariate Models for the Effect of Level of Glaucoma Damage on Log Half-Time

| Factor | Estimated Mean Half-Time | Regression Parameter Estimate (95% CI) | *P* Value | Categories Different at Adjusted $P \leq 0.05$ (Bonferroni) |
|---|---|---|---|---|
| Level of damage, 5 levels | | | | |
| Normal (R) | 1.902 | 0 | 0.02 | Normal, >50% |
| <10% | 2.176 | 0.134 (−0.148, 0.417) | | |
| 10%–25% | 2.424 | 0.242 (−0.162, 0.646) | | |
| 25%–50% | 2.549 | 0.292 (0.034, 0.551) | | |
| >50% | 2.884 | 0.402 (0.136, 0.669) | | |
| Level of damage, 3 levels | | | | |
| Normal (R) | 1.902 | 0 | 0.02 | Normal, ≥25% |
| <25% | 2.268 | 0.176 (−0.106, 0.458) | | |
| ≥25% | 2.664 | 0.337 (0.087, 0.586) | | |
| Level of damage, continuous, 0–4, per unit increase | ——— | 0.100 (0.029, 0.170) | 0.01 | ——— |

$N = 25$ eyes.

**Table 11.** Multivariable Models for the Effect of Level of Glaucoma Damage on Half-Time

| Factor | Regression Parameter Estimate (95% CI) | *P* Value From GEE Model | Categories Different at Adjusted $P \leq 0.05$ (Bonferroni) |
|---|---|---|---|
| Level of damage | | | |
| Normal | 0 | 0.004 | Normal, ≥25% |
| <25% | 0.029 (−0.156, 0.213) | | |
| ≥25% | 0.143 (0.042, 0.244) | | |
| Level of damage, continuous | 0.032 (0.004, 0.060) | 0.02 | |

Multivariable models, adjusted for strain and region.

to experimental glaucoma damage than younger CD1 mice.[42] Older CD1 mice have also longer eyes, which might logically lead to increased strain in the sclera, all other factors being equal. Yet, lower scleral permeability was associated here with those mouse strains less susceptible to glaucoma. It is likely that there are complex interactions involving the structural features of the sclera that contribute to glaucoma damage. These features are known to be altered by eye pressure through a biomechanical pathway. Thus, further studies are merited to dissect the features of scleral behavior that affect glaucoma damage.

We can consider what features of the scleral architecture determine permeability and how this might relate to susceptibility to glaucoma damage. In the same mouse strains studied here, Cone-Kimball et al.[16] have found that experimental glaucoma leads to a loss of nonfibrillar components of the sclera. In fact, the fibrillar, collagenous component of the sclera slightly increased in volume in these mice, as well as undergoing significant decreases in collagen fibril diameter. We have also determined that experimental mouse glaucoma leads to an increase in biomechanical stiffness of the sclera. Others have found that glaucomatous eyes in humans[1] and monkeys[43] are stiffer with glaucoma. Interestingly, inverse finite element modeling of the sclera in human glaucomatous eyes shows that the more significant change is in the component of sclera assigned to the nonfibrillar elements. Experiments with normal rabbit sclera indicate that permeability increases as hydration increases, that crosslinking of the sclera by glutaraldehyde reduces partition coefficients for solutes with molecular weights greater than 3 kDa, and that removal of glycosaminoglycans with chondroitinase has only a small effect on diffusion.[44] Our studies of scleral proteomics and composition will now be targeted to identify changes in the nonfibrillar elements, which may influence the stiffness as well as other functions of sclera as they impact glaucoma susceptibility.

The findings here may also have implications for the penetration and effects of topical glaucoma therapy and IOP. There is considerable evidence that drug and protein penetration of the sclera is measureable and potentially useful to produce clinically beneficial effects within the eye.[45–47] The scleral penetration of particles or agents in vivo is less than that in vitro,[48] suggesting a physiological barrier that may depend on re-absorption by blood vessels or lymphatics, or on uveoscleral outflow of aqueous from within to the outside of the sclera.[49,50] In vitro measurement of scleral permeability to water and large molecules decreases as IOP increases.[51] There may be regional differences in permeability between more anterior and more posterior sclera,[52] though specific studies of the peripapillary sclera have not been accomplished to our knowledge. Topical eyedrop medications can affect IOP either by penetrating the cornea to aqueous humor, or by passing through the conjunctiva and through the sclera. Interestingly, the prostaglandin analogues lower IOP not only by affecting trabecular outflow but also by increasing uveoscleral outflow, probably by altering metalloproteinase activity and increasing scleral permeability.[53]

The methods developed in this report have some limitations. The measurements of dextran molecular diffusion in the sclera are influenced by melanin pigment content in the tissues, which is most prominent in the peripapillary sclera of pigmented mice (B6). This may lead to some systematic differences in comparisons of control values between albino CD1 and B6, or between peripapillary sclera and more anterior regions. The peripapillary sclera of the mouse has several large channels through which blood vessels enter the eye. In performing our studies, we avoided these areas, and therefore collected more information from the superior peripapillary sclera. Standard methods using FRAP in single cells or very thin tissues can derive actual diffusivity measurements, estimating the pore size of the tissue of interest by comparing the half-time to recovery of fluorescence in the tissue to that in a fluid of equal thickness. Our scleral specimens are 50 to 100 μm thick and diffusion can occur not only from the lateral edges of the bleached zone, but also from unbleached tissue above and below the zone on which we focus by confocal microscopy. Thus, while our measurements are clearly consistent and highly related to tissue permeability, the present methods do no allow us to estimate tissue pore size. Finally, we have no immediate interpretation of the molecular mechanisms underlying either normal or pathological changes in diffusivity in the sclera. We plan extensive studies to explain the measured differences.

## *Acknowledgments*

Supported in part by Public Health Service Research Grants EY 02120 and EY 01765 (HAQ, and Wilmer Institute Core grant) and by unrestricted support from Saranne and Livingston Kosberg and William T. Forrester. The funders had no role in study design, data collection and analysis, decision to publish, or preparation of the manuscript.

Disclosure: **M.E. Pease**, None; **E.N. Oglesby**, None; **E. Cone-Kimball**, None; **J.L. Jefferys**, None; **M.R. Steinhart**, None; **A.J. Kim**, None; **J. Hanes**, None; **H.A. Quigley**, None

## *References*

1. Coudrillier B, Tian J, Alexander S, Myers KM, Quigley HA, Nguyen TD. Biomechanics of the human posterior sclera: age- and glaucoma-related changes measured using inflation testing. *Invest Ophthalmol Vis Sci*. 2012;53:1714–1728.
2. Anderson DR, Hendrickson A. Effect of intraocular pressure on rapid axoplasmic transport in monkey optic nerve. *Invest Ophthalmol*. 1974;13:771–783.
3. Quigley HA, Addicks EM, Green WR, Maumenee AE. Optic nerve damage in human glaucoma, II: the site of injury and susceptibility to damage. *Arch Ophthalmol*. 1981;99:635–649.

4. Sainz de la Maza M, Tauber J, Foster CS. The sclera. In: *Structural Considerations of the Sclera*. New York: Springer US; 2012:1–30.
5. Rada JAS, Shelton S, Norton TT. The sclera and myopia. *Exp Eye Res*. 2006;82:185–200.
6. Clark SJ, Keenan TDL, Fielder HL, et al. Mapping the differential distribution of glycosaminoglycans in the adult human retina, choroid, and sclera. *Invest Ophthalmol Vis Sci*. 2011;52:6511–6521.
7. Rada JA, Achen VR, Perry CA, Fox PW. Proteoglycans in the human sclera—evidence for the presence of aggrecan. *Invest Ophthalmol Vis Sci*. 1997;38:1740–1751.
8. Coudrillier B, Pijanka J, Jefferys J, et al. Age-related changes in the collagen structure and mechanical properties of the human sclera. *Biomech Model Mechanobiol*. In press.
9. Nguyen C, Cone FE, Nguyen TD, et al. Studies of scleral biomechanical behavior related to susceptibility for retinal ganglion cell loss in experimental mouse glaucoma. *Invest Ophthalmol Vis Sci*. 2013;54:1767–1780.
10. Downs JC, Blidner RA, Bellezza AJ, Thompson HW, Hart RT, Burgoyne CF. Peripapillary scleral thickness in perfusion-fixed normal monkey eyes. *Invest Ophthalmol Vis Sci*. 2002;43:2229–2235.
11. Olsen TW, Aaberg SY, Geroski DH, Edelhauser HF. Human sclera: thickness and surface area. *Am J Ophthalmol*. 1998;125:237–241.
12. Norman RE, Flanagan JG, Rausch SM, et al. Dimensions of the human sclera: thickness measurement and regional changes with axial length. *Exp Eye Res*. 2010;90:277–284.
13. Quigley HA, Dorman-Pease ME, Brown AE. Quantitative study of collagen and elastin of the optic nerve head and sclera in human and experimental monkey glaucoma. *Curr Eye Res*. 1991;10:877–888.
14. Hogan MJ, Alvarado JA, Weddell JE. The sclera. *Histology of the Human Eye*. Philadelphia, PA: W. B. Saunders Co. 1971;193–200.
15. Anderson DR. Ultrastructure of human and monkey lamina cribrosa and optic nerve head. *Arch Ophthalmol*. 1969;82:800–814.
16. Cone-Kimball E, Nguyen C, Oglesby EN, Pease ME, Steinhart MR, Quigley HA. Scleral structural alterations associated with chronic experimental IOP elevation in mice. *Mol Vis*. 2013;19:2023–2039.
17. Hernandez MR, Luo XX, Igoe F, Neufeld AH. Extracellular matrix of the human lamina cribrosa. *Am J Ophthalmol*. 1987;104:567–576.
18. Quigley HA, Brown A, Dorman-Pease ME. Alterations in elastin of the optic nerve head in human and experimental glaucoma. *Br J Ophthalmol*. 1991;75:552–557.
19. Yan D, McPheeters S, Johnson G, Utzinger U, Vande Geest JP. Microstructural differences in the human posterior sclera as a function of age and race. *Invest Ophthalmol Vis Sci*. 2011;52:821–829.
20. Pijanka JK, Coudrillier B, Ziegler K, et al. Quantitative mapping of collagen fiber orientation in non-glaucoma and glaucoma posterior human sclerae. *Invest Ophthalmol Vis Sci*. 2012;53:5258–5270.
21. Gelman S, Cone FE, Pease ME, Nguyen TD, Myers K, Quigley HA. The presence and distribution of elastin in the posterior and retrobulbar regions of the mouse eye. *Exp Eye Res*. 2010;90:210–215.
22. Girard MJA, Dahlmann-Noor A, Rayapureddi S, et al. Quantitative mapping of scleral fiber orientation in normal rat eyes. *Invest Ophthalmol Vis Sci*. 2011;52:9684–9693.
23. Girard MJA, Suh J-KF, Bottlang M, Burgoyne CF, Downs JC. Scleral biomechanics in the aging monkey eye. *Invest Ophthalmol Vis Sci*. 2009;50:5226–5237.
24. McBrien NA, Cornell LM, Gentle A. Structural and ultrastructural changes to the sclera in a mammalian model of high myopia. *Invest Ophthalmol Vis Sci*. 2001;42:2179–2187.
25. Wiesel TN, Raviola E. Myopia and eye enlargement after neonatal lid fusion in monkeys. *Nature*. 1977;266:66–68.
26. Backhouse S, Phillips JR. Effect of induced myopia on scleral myofibroblasts and in vivo ocular biomechanical compliance in the guinea pig. *Invest Ophthalmol Vis Sci*. 2010;51:6162–6171.
27. McBrien NA, Lawlor P, Gentle A. Scleral remodeling during the development of and recovery from axial myopia in the tree shrew. *Invest Ophthalmol Vis Sci*. 2000;41:3713–3719.
28. Tejedor J, de la Villa P. Refractive changes induced by form deprivation in the mouse eye. *Invest Ophthalmol Vis Sci*. 2003;44:32–36.
29. Burgoyne CF, Downs JC, Bellezza AJ, Suh J-KF, Hart RT. The optic nerve head as a biomechanical structure: a new paradigm for understanding the role of IOP-related stress and strain in the pathophysiology of glaucomatous optic nerve head damage. *Prog Ret Eye Res*. 2005;24:39–73.
30. Puk O, Dalke C, Calzada-Wack J, et al. Reduced corneal thickness and enlarged anterior chamber in a novel Col-VIIIa2G257D mutant mouse. *Invest Ophthalmol Vis Sci*. 2009;50:5653–5661.
31. Steinhart MR, Cone FE, Nguyen C, et al. Mice with an induced mutation in cllagen 8A2 develop larger eyes and are resistant to retinal ganglion cell damage in an experimental glaucoma model. *Mol Vis*. 2012;18:1093–1106.
32. Cone FE, Gelman SE, Son JL, Pease ME, Quigley HA. Differential susceptibility to experimental glaucoma among 3 mouse strains using bead and viscoelastic injection. *Exp Eye Res*. 2010;91:415–424.
33. Cone FE, Steinhart MR, Oglesby EN, Kalesnykas G, Pease ME, Quigley HA. The effects of anesthesia, mouse strain and age on intraocular pressure and an improved murine model of experimental glaucoma. *Exp Eye Res*. 2012;99:27–35.
34. Hadi MF, Sander EA, Ruberti JW, Barocas VH. Simulated remodeling of loaded collagen networks via strain-dependent enzymatic degradation and constant-rate fiber growth. *Mech Mater*. 2012;44:72–82.
35. Axelrod D, Koppel DE, Schlessinger J, Elson E, Webb WW. Mobility measurement by analysis of fluorescence photobleaching recovery kinetics. *Biophys J*. 1976;16:1055–1069.
36. Danysh BP, Patel TP, Czymmek KJ, et al. Characterizing molecular diffusion in the lens capsule. *Matrix Biol*. 2010;29:228–236.
37. Morrison JC. Elevated intraocular pressure and optic nerve injury models in the rat. *J Glaucoma*. 2005;14:315–317.
38. Sigal IA, Flanagan JG, Etheir CR. Factors influencing optic nerve head biomechanics. *Invest Ophthalmol Vis Sci*. 2005;46:4189–4199.
39. Boland MV, Quigley HA. Risk factors and open-angle glaucoma: concepts and applications. *J Glaucoma*. 2007;16:406–418.
40. Jackson TL, Hussain, A, Hodgetts A, et al. Human scleral hydraulic conductivity: age-related changes, topographical variation, and potential scleral outflow facility. *Invest Ophthalmol Vis Sci*. 2006;47:4942–4946.
41. Anderson OA, Jackson TL, Singh JK, Hussain AA, Marshall J. Human transscleral albumin permeability and the effect of topographical location and donor age. *Invest Ophthalmol Vis Sci*. 2008;49:4041–4045.
42. Steinhart MR, Cone-Kimball E, Nguyen C, et al. Susceptibility to glaucoma damage related to age and connective tissue mutations in mice. *Exp Eye Res*. 2013;119C:54–60.
43. Girard MJA, Suh J-KF, Mottlang M, Burgoyne CF, Downs JC. Biomechanical changes in the sclera of monkey eyes exposed

to chronic IOP elevations. *Invest Ophthamol Vis Sci*. 2011;52: 5656–5669.

44. Boubriak OA, Urban JP, Akhtar S, Meek KM, Bron AJ. The effect of hydration and matrix composition on solute diffusion in rabbit sclera. *Exp Eye Res*. 2000;71:503–514.
45. Geroski DH, Henry F, Edelhauser HF. Transscleral drug delivery for posterior segment disease. *Adv Drug Deliv Rev*. 2001;52: 37–48.
46. Ambati J, Canakis CS, Miller JW, et al. Diffusion of high molecular weight compounds through sclera. *Invest Ophthalmol Vis Sci*. 2000;41:1181–1185.
47. Amaral J, Fariss RN, Campos MM, et al. Transscleral-RPE permeability of PEDF and ovalbumin proteins: implications for subconjunctival protein delivery. *Invest Ophthalmol Vis Sci*. 2005;46:4383–4392.
48. Amrite AC, Edelhauser HF, Singh SR, Kompella UB. Effect of circulation on the disposition and ocular tissue distribution of 20 nm nanoparticles after periocular administration. *Mol Vis*. 2008;14:150–160.
49. Bill A. The drainage of albumin from the uvea. *Exp Eye Res*. 1964;3:179–187.
50. Emi K, Pederson JE, Toris CB. Hydrostatic pressure of the suprachoroidal space. *Invest Ophthalmol Vis Sci*. 1989;30: 233–238.
51. Rudnick DE, Noonan JS, Geroski DH, Prausnitz MR, Edelhauser HF. The effect of intraocular pressure on human and rabbit scleral permeability. *Invest Ophthalmol Vis Sci*. 1999;40: 3054–3058.
52. Boubriak OA, Urban JP, Bron AJ. Differential effects of aging on transport properties of anterior and posterior human sclera. *Exp Eye Res*. 2003;76:701–713.
53. Weinreb RN. Enhancement of scleral macromolecular permeability with prostaglandins. *Trans Am Ophthalmol Soc*. 2001; 99:319–343.

Investigative Ophthalmology & Visual Science